

Article

# Phenoxazine-Dibenzothiophene Sulfoximine Emitters Featuring Both Thermally Activated Delayed Fluorescence and Aggregation Induced Emission

Yiyu Yang <sup>1,2</sup>, Ran Xiao <sup>1,2</sup>, Xiaosong Cao <sup>1,\*</sup>, Zhanxiang Chen <sup>3</sup>, Xialei Lv <sup>1</sup>, Youming Zhang <sup>1,\*</sup>, Shaolong Gong <sup>3</sup>, Yang Zou <sup>1</sup> and Chuluo Yang <sup>1,3</sup>

- <sup>1</sup> Shenzhen Key Laboratory of Polymer Science and Technology, College of Materials Science and Engineering, Shenzhen University, Shenzhen 518060, China; 1910342080@email.szu.edu.cn (Y.Y.); xiaoran@szu.edu.cn (R.X.); lvxl0907@163.com (X.L.); yangzou@szu.edu.cn (Y.Z.); clyang@szu.edu.cn (C.Y.)
- <sup>2</sup> Key Laboratory of Optoelectronic Devices and Systems of Ministry of Education and Guangdong Province, College of Optoelectronic Engineering, Shenzhen University, Shenzhen 518060, China
- <sup>3</sup> Hubei Key Lab on Organic and Polymeric Optoelectronic Materials, Department of Chemistry, Wuhan University, Wuhan 430072, China; zhanxiangchen@whu.edu.cn (Z.C.); slgong@whu.edu.cn (S.G.)
- \* Correspondence: xcao@szu.edu.cn (X.C.); zhangyouming1218@126.com (Y.Z.)

**Abstract:** In this work, we demonstrate dibenzothiophene sulfoximine derivatives as building blocks for constructing emitters featuring both thermally activated delayed fluorescent (TADF) and aggregation-induced emission (AIE) properties, with multiple advantages including high chemical and thermal stability, facile functionalization, as well as tunable electron-accepting ability. A series of phenoxazine-dibenzothiophene sulfoximine structured TADF emitters were successfully synthesized and their photophysical and electroluminescent properties were evaluated. The electroluminescence devices based on these emitters displayed diverse emissions from yellow to orange and reached external quantum efficiencies (EQEs) of 5.8% with 16.7% efficiency roll-off at a high brightness of 1000 cd·m<sup>-2</sup>.

**Keywords:** organic light-emitting diodes; thermally activated delayed fluorescence; color-managing acceptor; aggregation induced emission

**Citation:** Yang, Y.; Xiao, R.; Cao, X.; Chen, Z.; Lv, X.; Zhang, Y.; Gong, S.; Zou, Y.; Yang, C. Phenoxazine-Dibenzothiophene Sulfoximine Emitters Featuring Both Thermally Activated Delayed Fluorescence and Aggregation Induced Emission. *Molecules* **2021**, *26*, 5243. <https://doi.org/10.3390/molecules26175243>

Academic Editor: Pradip K. Bhowmik

Received: 31 July 2021  
Accepted: 24 August 2021  
Published: 29 August 2021

**Publisher's Note:** MDPI stays neutral with regard to jurisdictional claims in published maps and institutional affiliations.



**Copyright:** © 2021 by the authors. Licensee MDPI, Basel, Switzerland. This article is an open access article distributed under the terms and conditions of the Creative Commons Attribution (CC BY) license (<http://creativecommons.org/licenses/by/4.0/>).

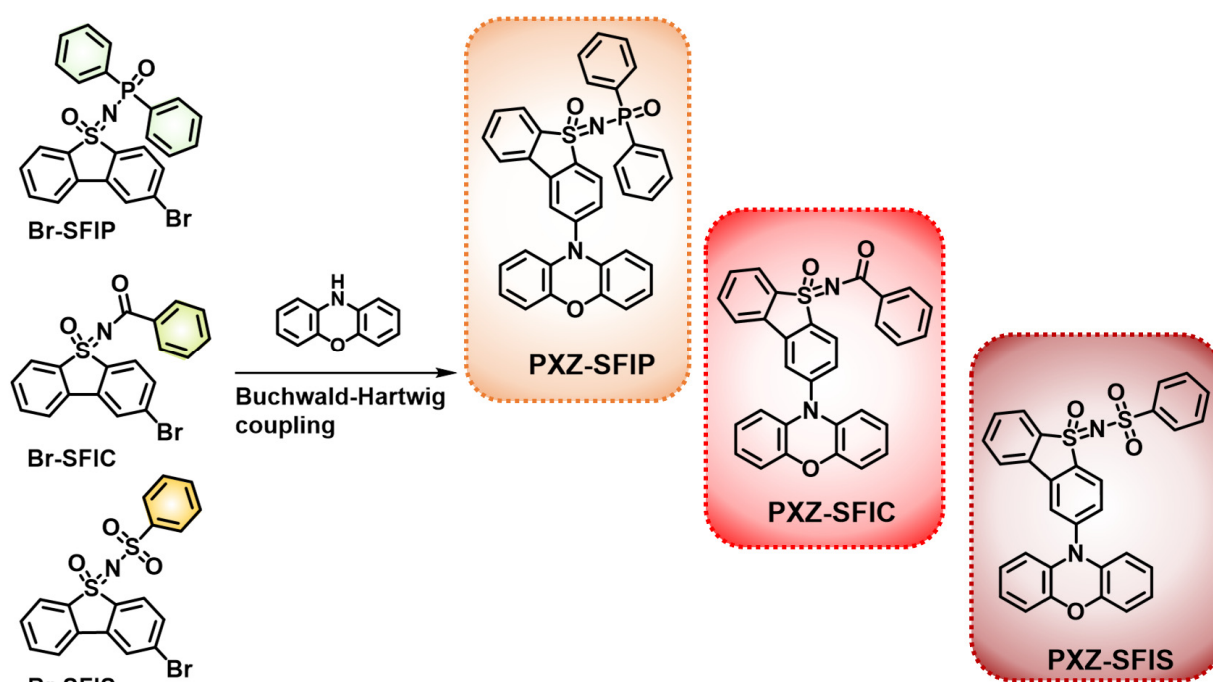
## 1. Introduction

Materials with thermally activated delayed fluorescence (TADF) have been extensively explored since the pioneering research by Adachi et al. [1]. Due to the merits of diverse emission colors, high efficiency, and low cost, TADF molecules are highly potent in next-generation solid lighting and display devices [2–6]. Mechanistically, the theoretical 100% internal quantum efficiency (IQE) of organic light-emitting diodes (OLEDs) based on TADF emitters is enabled by efficient reverse intersystem crossing (RISC) of the triplet excitons to singlet excited states [7–11]. To facilitate up-conversion of triplet excitons, a small energy splitting ( $\Delta E_{ST}$ , below 0.2 eV) between singlet ( $S_1$ ) and triplet ( $T_1$ ) excited states is required [12,13]. The predominant strategy is the spatial separation of the highest occupied molecular orbital (HOMO) and the lowest unoccupied molecular orbital (LUMO) with twisted donor-acceptor (D-A) linkage to effectively reduce the exchange integral of the orbitals [14–17].

For TADF emitters with prominent intramolecular charge-transfer (ICT) characters, careful selection of electron-donating or -accepting units allows delicate manipulation of emission colors [18–22]. On the other side, improvements in device performance also heavily rely on judicious molecular design guided by structure–property relationship in-

vestigations [23–25]. Currently, it has been demonstrated by numerous reports that conjugation of nitrogen-containing aromatics (i.e., carbazole [26], dimethylacridane [27], phenoxazine [28,29]) with acceptors such as aza-aromatic rings [15–19], ketones [29–31], nitriles [32–34], sulfones [35–37], boranes [38,39], amides [40], could realize decent device efficiencies. However, the majority of these structural units are chemically inert and not easy to be functionalized, disfavoring color management or further optimization of device performances.

Sulfoximines are monoaza analogs of sulfones featuring high stability and versatile chemistry that have been widely studied in the pharmaceutical field [41,42]. Apart from that, the mild basic nitrogen atom in sulfoximine provides the possibility for facile chemical functionalization [43]. In this way, the photophysical properties could be easily adjusted by tuning the electron-withdrawing ability of the functionalized sulfoximines using appropriate *N*-substitutes [44]. In this work, we report three TADF fluorophores with aggregation-induced emission (AIE) character using dibenzothiophene sulfoximine with different *N*-functional units as an acceptor and 10*H*-phenoxazine (PXZ) as a donor. These emitters were denoted as **PXZ-SFIP**, **PXZ-SFIC**, **PXZ-SFIS**, with the NH site substituted by diphenylphosphoryl, benzoyl, and benzenesulfonyl groups, respectively, as shown in Scheme 1. The facile metal-free functionalization of dibenzothiophene sulfoximine provides delicate control of electron deficiency of the acceptors and regulates the overall photophysical performance. OLEDs fabricated with these TADF emitters as a dopant in emitting layer obtained diverse electroluminescence (EL) from yellow to orange, with a maximum external quantum efficiency (EQE<sub>max</sub>) exceeding 5%, and insignificant efficiency roll-off of 16.7% at a high brightness of 1000 cd m<sup>-2</sup>, demonstrating the phenoxazine-dibenzothiophene sulfoximine compounds as promising emitters for TADF-OLEDs.



**Scheme 1.** Synthesis route of the TADF emitters with functionalized dibenzothiophene sulfoximine-type acceptor.

## 2. Experimental Section

### 2.1. Materials

All starting chemicals and reagents were purchased from commercial suppliers and used without further purification.

### 2.2. General Information

The Fourier-transformed infrared spectra (FT-IR) were recorded on a Thermo Nicolet 6700 Spectrometer. The  $^1\text{H}$  and  $^{13}\text{C}$  nuclear magnetic resonance (NMR) spectra were collected in dilute  $\text{CDCl}_3$  solution at 25 °C on a Bruker AVANCE III 500 superconducting-magnet high-field NMR spectrometer at 500 MHz and 126 MHz, respectively, using tetramethylsilane (TMS) as an internal standard. Thermogravimetric analysis (TGA) was carried out with a TA instrument TGA Q50 under nitrogen flow ( $20 \text{ mL}\cdot\text{min}^{-1}$ ), and differential scanning calorimetry (DSC) was performed with a TA DSC Q200 under nitrogen. The glass transition temperature ( $T_g$ ) was determined from the second heating scan. UV-Vis absorption spectra were recorded on a Shimadzu UV-2700 recording spectrophotometer. Photoluminescence (PL) spectra were recorded on a Hitachi F-4600 fluorescence spectrophotometer. Phosphorescence spectra of doped thin films were conducted at 77 K. The transient photoluminescence decay curves were measured by a single photon counting spectrometer from Edinburgh Instruments (FLS920) with a Picosecond Pulsed UV-LASTER (LASTER377) as the excitation source. The photoluminescence quantum efficiencies were measured using an absolute photoluminescence quantum yield measurement system (C9920-02, Hamamatsu Photonics).

Cyclic voltammetry (CV) was carried out in nitrogen-purged dichloromethane at room temperature with a CHI voltammetric analyzer. Tetrabutylammonium hexafluorophosphate (0.1 M) was used as the supporting electrolyte. The conventional three-electrode configuration consisted of a platinum working electrode, a platinum wire auxiliary electrode, and an  $\text{Ag}/\text{Ag}^+$  reference electrode with ferrocenium ferrocene ( $\text{Fc}^+/\text{Fc}$ ) as the internal standard. Cyclic voltammograms were obtained at a scan rate of 100 mV/s. Formal potentials were calculated as the average of cyclic voltammetric anodic and cathodic peaks. The HOMO energy levels of the compounds were calculated according to the formula:  $-[4.8 + (E_{1/2(\text{ox/red})} - E_{1/2(\text{Fc/Fc}^+)})]$  eV. The LUMO energy levels of the compounds were calculated according to the HOMO values and the absorption on-set of the longer wavelength.

### 2.3. Synthesis

#### General Synthetic Procedures of the TADF Molecules

To a pre-dried 50 mL twin-neck round-bottom flask, Br-SFIP/Br-SFIC/Br-SFIS precursor (1.0 eq), 10*H*-phenoxazine (PXZ, 1.2 eq), palladium acetate (0.1 eq), tri-*tert*-butylphosphonium tetrafluoroborate (0.2 eq) and cesium carbonate (2.5 eq) were added together with a magnetic stirrer. The flask was evacuated and back-filled with argon for three cycles. Anhydrous toluene (10 mL) was then injected under argon flow via syringe. After refluxing for 36 h, the solvent was evaporated, and then purified by silica gel chromatography (hexanes/ethyl acetate, 8:1 *v/v* in all cases).

#### 2.3.1. PXZ-SFIP.

Synthesized from compound **Br-SFIP** (0.50 g, 1.01 mmol). 0.57 g, 0.91 mmol yellowish orange solid, 84% yield. FT-IR:  $\nu_{\text{max}} = 3056, 1588, 1439, 1325, 1244, 1121, 1050, 736, 692, 654, 514 \text{ cm}^{-1}$ .  $^1\text{H}$  NMR (500 MHz,  $\text{CDCl}_3$ )  $\delta$  (ppm): 8.30 (d,  $J = 8.1 \text{ Hz}$ , 1H), 8.07 (d,  $J = 7.7 \text{ Hz}$ , 1H), 7.89–7.76 (m, 4H), 7.76–7.67 (m, 2H), 7.63 (td,  $J = 7.5, 1.2 \text{ Hz}$ , 1H), 7.56 (td,  $J = 7.6, 1.1 \text{ Hz}$ , 1H), 7.48–7.28 (m, 7H), 6.77–6.68 (m, 4H), 6.64 (td,  $J = 7.6, 1.9 \text{ Hz}$ , 2H), 5.97 (dd,  $J = 8.0, 1.3 \text{ Hz}$ , 2H).  $^{13}\text{C}$  NMR (126 MHz,  $\text{CDCl}_3$ )  $\delta$  (ppm): 144.67, 143.98, 139.56 (d,  $J = 3.7 \text{ Hz}$ ), 138.51 (d,  $J = 2.7 \text{ Hz}$ ), 135.51 (d,  $J = 132.2 \text{ Hz}$ ), 135.22 (d,  $J = 132.8 \text{ Hz}$ ), 135.15, 134.06, 133.32, 133.06, 131.34 (d,  $J = 3.0 \text{ Hz}$ ), 131.30 (d,  $J = 3.3 \text{ Hz}$ ), 131.18 (d,  $J = 10.7 \text{ Hz}$ ), 131.14 (d,  $J = 10.1 \text{ Hz}$ ), 131.12, 130.68, 128.28 (d,  $J = 3.8 \text{ Hz}$ ), 128.17 (d,  $J = 3.3 \text{ Hz}$ ), 126.70, 123.99, 123.61, 123.45, 122.29, 121.82, 115.93, 113.51.

#### 2.3.2. PXZ-SFIC.

Synthesized from compound **Br-SFIC** (0.50 g, 1.01 mmol). 0.57 g, 0.91 mmol orange solid, 88% yield. FT-IR:  $\nu_{\text{max}} = 3058, 1621, 1582, 1482, 1323, 1264, 1217, 1123, 928, 827, 707,$

633, 545  $\text{cm}^{-1}$ .  $^1\text{H}$  NMR (500 MHz,  $\text{CDCl}_3$ )  $\delta$  (ppm): 8.64 (d,  $J = 8.2$  Hz, 1H), 8.39–8.34 (m, 1H), 8.21–8.12 (m, 2H), 7.86 (d,  $J = 1.8$  Hz, 1H), 7.81 (d,  $J = 7.6$  Hz, 1H), 7.73 (td,  $J = 7.6, 1.2$  Hz, 1H), 7.66 (td,  $J = 7.6, 1.1$  Hz, 1H), 7.60 (dd,  $J = 8.1, 1.8$  Hz, 1H), 7.54–7.48 (m, 1H), 7.44–7.36 (m, 2H), 6.79–6.69 (m, 4H), 6.65 (td,  $J = 7.6, 1.8$  Hz, 2H), 6.06 (dd,  $J = 8.0, 1.4$  Hz, 2H).  $^{13}\text{C}$  NMR (126 MHz,  $\text{CDCl}_3$ )  $\delta$  (ppm): 175.22, 145.46, 144.02, 137.55, 136.55, 136.50, 134.84, 134.61, 133.28, 133.25, 132.52, 132.07, 131.31, 129.65, 128.76, 128.12, 125.61, 124.26, 123.48, 122.39, 122.06, 115.99, 113.56.

### 2.3.3. PXZ-SFIS.

Synthesized from compound **Br-SFIS** (0.50 g, 1.01 mmol). 0.57 g, 0.91 mmol red solid, 65% yield. FT-IR:  $\nu_{\text{max}} = 3059, 1582, 1486, 1328, 1312, 1273, 1230, 1150, 1077, 1032, 731, 686, 630, 538$   $\text{cm}^{-1}$ .  $^1\text{H}$  NMR (500 MHz,  $\text{CDCl}_3$ )  $\delta$  (ppm): 8.39 (d,  $J = 8.2$  Hz, 1H), 8.16 (d,  $J = 7.8$  Hz, 1H), 8.13–8.07 (m, 2H), 7.83 (d,  $J = 1.8$  Hz, 1H), 7.78 (d,  $J = 7.6$  Hz, 1H), 7.72 (td,  $J = 7.6, 1.1$  Hz, 1H), 7.65–7.50 (m, 5H), 6.81–6.72 (m, 4H), 6.67 (ddd,  $J = 8.8, 7.1, 2.0$  Hz, 2H), 6.04 (dd,  $J = 8.0, 1.3$  Hz, 2H).  $^{13}\text{C}$  NMR (126 MHz,  $\text{CDCl}_3$ )  $\delta$  (ppm): 145.99, 144.08, 143.23, 137.13, 136.08, 135.99, 135.06, 133.33, 133.09, 132.54, 131.54, 131.45, 128.85, 127.95, 126.85, 125.18, 124.18, 123.51, 122.56, 122.07, 116.08, 113.63.

## 2.4. Fabrication and Characterization of Devices

The ITO coated glass substrates with a sheet resistance of  $15 \Omega \text{ square}^{-1}$  were consecutively ultrasonicated with acetone/ethanol and dried with nitrogen gas flow, followed by 20 min ultraviolet light-ozone (UVO) treatment in a UV-ozone surface processor (PL16 series, Sen Lights Corporation). Then, the sample was transferred to the deposition system. All organic layers were deposited at a rate of  $1 \text{ \AA s}^{-1}$ , and subsequently, Liq was deposited at  $0.2 \text{ \AA s}^{-1}$  and then capped with Al (ca.  $4 \text{ \AA s}^{-1}$ ) through a shadow mask in a vacuum of  $2 \times 10^{-5}$  mbar. For all the OLEDs, the emitting areas were determined by the overlap of two electrodes as  $0.09 \text{ cm}^2$ . The as-fabricated devices were measured in an ambient environment without any encapsulation. The EL spectra and Commission Internationale de l'Eclairage (CIE) coordinates were recorded with a Keithley 2400 source meter unit. The current density-voltage-luminance ( $J$ - $V$ - $L$ ) curves of the devices were measured with a PHOTO RESEARCH SpectraScan PR 735 spectrometer. The EQE was calculated from the current density, luminance, and EL (electroluminescence) spectrum, assuming a Lambertian distribution.

## 3. Results and Discussions.

### 3.1. Synthesis and Characterization

The Br-SFIP/Br-SFIC/Br-SFIS compounds were prepared according to the previously reported procedure [45]. The donor unit 10H-phenoxazine was connected to the Br-SFIX precursor via Buchwald–Hartwig coupling. The  $^1\text{H}$  NMR and  $^{13}\text{C}$  NMR spectra were in good agreement with the structure of the TADF molecules of **PXZ-SFIP**, **PXZ-SFIC**, and **PXZ-SFIS**.

### 3.2. Thermal and Electrochemical Properties

Thermogravimetric analysis (TGA) and differential scanning calorimetry (DSC) were employed to investigate the thermal properties of the TADF compounds. High decomposition temperatures ( $T_{\text{as}}$ : corresponding to the temperature at 5% weight loss) of 350, 320, and 355  $^{\circ}\text{C}$  were recorded for **PXZ-SFIP**, **PXZ-SFIC**, and **PXZ-SFIS**, respectively (see ESI, Figure S1). Meanwhile, the emitters presented sufficient high glass transition temperatures ( $T_{\text{gs}}$ ) to prevent crystallization upon operation of the devices, as indicated by DSC measurements, where **PXZ-SFIC** presented the highest  $T_{\text{g}}$  value of 117  $^{\circ}\text{C}$ , comparing to that of 109  $^{\circ}\text{C}$  for **PXZ-SFIP** and 98  $^{\circ}\text{C}$  for **PXZ-SFIS** (see ESI, Figure S2). To study the electrochemical properties of the designed TADF compounds, cyclic voltammetry was performed (Figure S3). The HOMO levels of the emitters were estimated to be  $\sim -5.19$  eV

for all cases, reflecting comparable oxidation potential arising from PXZ electron-donating units. (Table 1).

**Table 1.** Calculated photophysical parameters of the designed emitters.

| Entry    | LUMO<br>(eV) | HOMO<br>(eV) | $E_g$<br>(eV) | $S_1$<br>(eV) | $T_1$<br>(eV) | $\Delta E_{ST}$<br>(eV) |
|----------|--------------|--------------|---------------|---------------|---------------|-------------------------|
| PXZ-SFIP | -2.23        | -4.97        | 2.74          | 2.38          | 2.29          | 0.08                    |
| PXZ-SFIC | -2.39        | -5.08        | 2.69          | 2.32          | 2.29          | 0.03                    |
| PXZ-SFIS | -2.58        | -5.26        | 2.68          | 2.29          | 2.26          | 0.02                    |

### 3.3. Theoretical Calculation

Density functional theory (DFT) calculations at the B3LYP-D3(BJ)/def2-SVP level were carried out to reveal the optimized ground-state geometries and the electronic structures of the designed emitters. As shown in Figure 1, the dihedral angles between the PXZ donor planes and the adjacent dibenzothiophene sulfoximine moieties were measured to be 78.5°, 85.6°, and 85.4° in **PXZ-SFIP**, **PXZ-SFIC**, and **PXZ-SFIS**, respectively, leading to nearly complete separation of the frontier molecular orbitals (FMOs). The diphenylphosphoryl, benzoyl, and benzenesulfonyl substituted dibenzothiophene sulfoximines exhibited a trend of increased electron-withdrawing ability, demonstrated by gradually deepened LUMO levels of -2.23 eV for **PXZ-SFIP**, -2.39 eV for **PXZ-SFIC**, and -2.58 eV for **PXZ-SFIS** in sequence. The energy gaps between HOMO and LUMO of the three compounds were calculated to be 2.74 eV, 2.69 eV, and 2.68 eV, respectively, as depicted in Figure 1.

The natural transition orbitals (NTO) patterns were investigated to describe the properties of the excited states of the molecules. Time-dependent DFT (TD-DFT) was performed at PBE0-D3(BJ)/def2-SVP level on the basis of the optimized ground-state geometries. Both  $S_1$  and  $T_1$  states were typical CT excited states with the ‘hole’ located on the donor moieties, and the ‘particles’ resided on the dibenzothiophene sulfoximines. The  $S_1/T_1$  levels of **PXZ-SFIP** (2.38/2.29 eV), **PXZ-SFIC** (2.32/2.29 eV), and those of **PXZ-SFIS** (2.29/2.26 eV) guaranteed relatively small  $\Delta E_{ST}$ s for effective thermally activated RISC processes (Table 1). Meanwhile, the oscillator strengths ( $f$ ) from  $S_0 \rightarrow S_1$  were calculated to be 0.0177, 0.0028, and 0.0001 for **PXZ-SFIP**, **PXZ-SFIC**, and **PXZ-SFIS**, respectively, predicting a higher singlet radiative transition rate ( $k_{r,s}$ ) of **PXZ-SFIP** due to the presence of small yet adequate overlap between its FMOs. The corresponding information is summarized in Table S1.

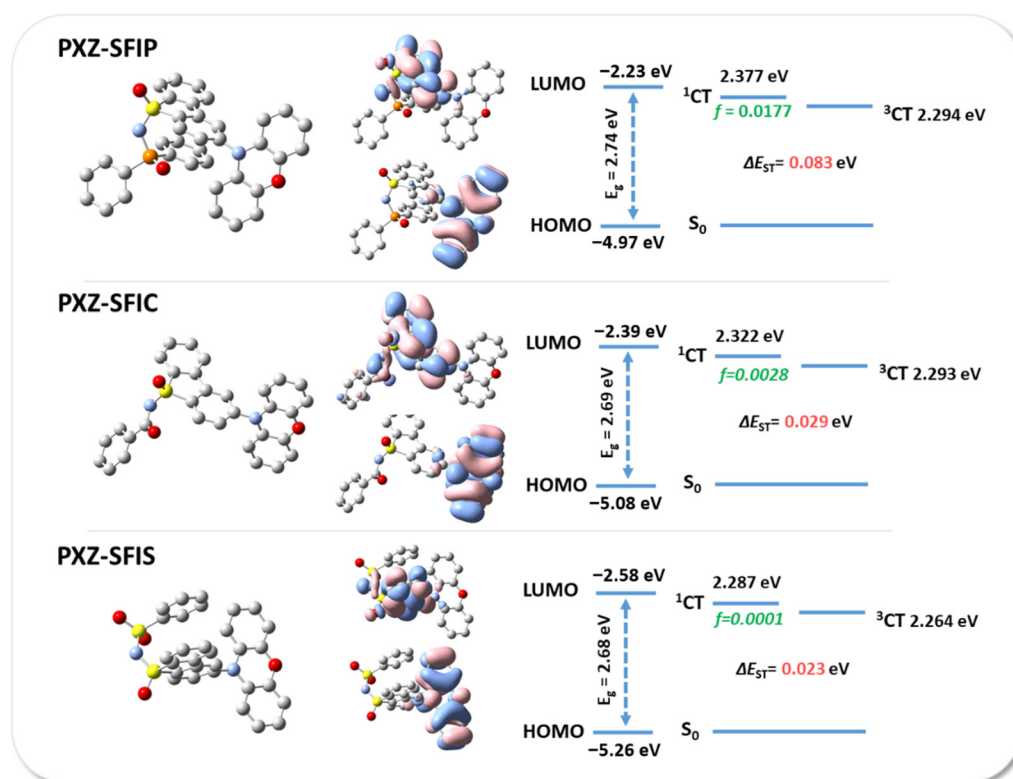


**Figure 1.** Optimized conformation, frontier orbital distributions, and theoretical calculated energy levels of ground states and excited states of the proposed PXZ-SFIP, PXZ-SFIC, and PXZ-SFIS compounds.

### 3.4. Photophysical Properties

The UV-Vis absorption spectra of the TADF compounds in dilute toluene solutions ( $10^{-5}$  mol·L $^{-1}$ ) are exhibited in Figure 2. The bands below 350 nm with high intensity were ascribed to  $\pi$ - $\pi^*$  absorption from the conjugated skeleton, while the broad structureless bands peaking at 400~430 nm represented characteristic intramolecular charge transfer (ICT) transition from the phenoxazine to dibenzothiophene sulfoximine unit. Upon excitation, the PXZ-SFIP, PXZ-SFIC, and PXZ-SFIS compounds revealed fluorescence with singular Gaussian-shaped emission bands, peaking at 576 nm, 574 nm, and 611 nm, respectively. Amongst three emitters, PXZ-SFIS, acquiring more electron-deficient benzenesulfonyl substitution on imine, caused a larger Stokes shift with red-shifted emission, while the emission bands of PXZ-SFIP and PXZ-SFIC were nearly overlapping with each other. Optical bandgaps of the emitters were 2.60 eV, 2.54 eV, and 2.49 eV, separately, as estimated from the onset of the absorption spectra from the longer wavelength. The decreasing optical bandgap corresponded well with increasing electron deficiency of the functionalized dibenzothiophene sulfoximine, giving deepening LUMO levels of -2.59 eV for PXZ-SFIP, -2.64 eV for PXZ-SFIC, and -2.70 eV for PXZ-SFIS (Table 2).

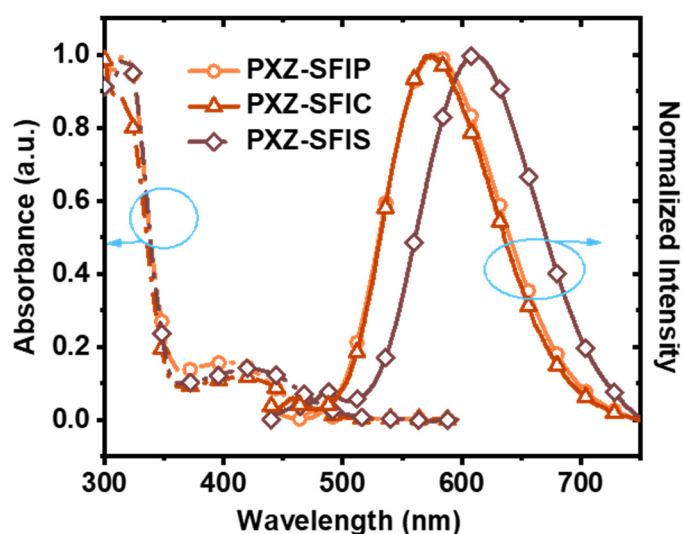


**Figure 2.** Absorption (Abs.) and emission (Fl.) spectra of PXZ-SFIP, PXZ-SFIC, and PXZ-SFIS ( $10^{-5}$  M) measured at room temperature in toluene.

**Table 2.** Photophysical properties of the TADF emitters.

| Compound | $\lambda_{\text{abs}}^a$ (nm) | $\lambda_{\text{em}}^a$ (nm) | $\lambda_{\text{em}}^b$ (nm) | $E_g^c$ (eV) | HOMO <sup>d</sup> /LUMO <sup>e</sup> (eV) | $S_1^f/T_1^g$ (eV) | $\Delta E_{ST}$ (eV) |
|----------|-------------------------------|------------------------------|------------------------------|--------------|---|--------------------|----------------------|
| PXZ-SFIP | 317/403                       | 576                          | 539                          | 2.60         | -5.19/-2.59                               | 2.61/2.59          | 0.02                 |
| PXZ-SFIC | 313/413                       | 574                          | 556                          | 2.54         | -5.18/-2.64                               | 2.54/2.52          | 0.02                 |
| PXZ-SFIS | 318/421                       | 611                          | 568                          | 2.49         | -5.19/-2.70                               | 2.51/2.48          | 0.03                 |

<sup>a</sup> Measured in toluene solution ( $10^{-5}$  M) at room temperature; <sup>b</sup> Measured in the doped films with TADF emitters in CBP host (10 wt%); <sup>c</sup> Estimated by the onset of the UV-vis spectra from longer wavelengths; <sup>d</sup> Determined by the onset of the oxidation potentials and <sup>e</sup> HOMO minus optical energy gaps calculated from the onset of UV-Vis spectra. <sup>f</sup> Estimated from the onset of low-temperature fluorescent and <sup>g</sup> phosphorescent spectra of doped films with TADF emitters in CBP host (10 wt%).

AIE characteristics of the PXZ-SFIP, PXZ-SFIC, and PXZ-SFIS compounds in THF/water mixed solvents with different water fractions ( $f_w$ ) were investigated, as shown in Figure 3 and Figure S4. In solutions with  $f_w$  lower than 80%, the fully dissolved emitters were almost non-emissive where peripheral functional groups could freely rotate and dissipate energy. Further increasing  $f_w$  led to a significant increase in PL intensities by the formation of aggregates, as explained by the restriction of intramolecular rotation (RIR) of the TADF emitter [45]. This distinct AIE behavior was beneficial for solid-state emission due to the suppression of undesirable aggregation-caused quenching (ACQ), which could potentially improve device performances and alleviate undesirable efficiency roll-off at high brightness in OLEDs.

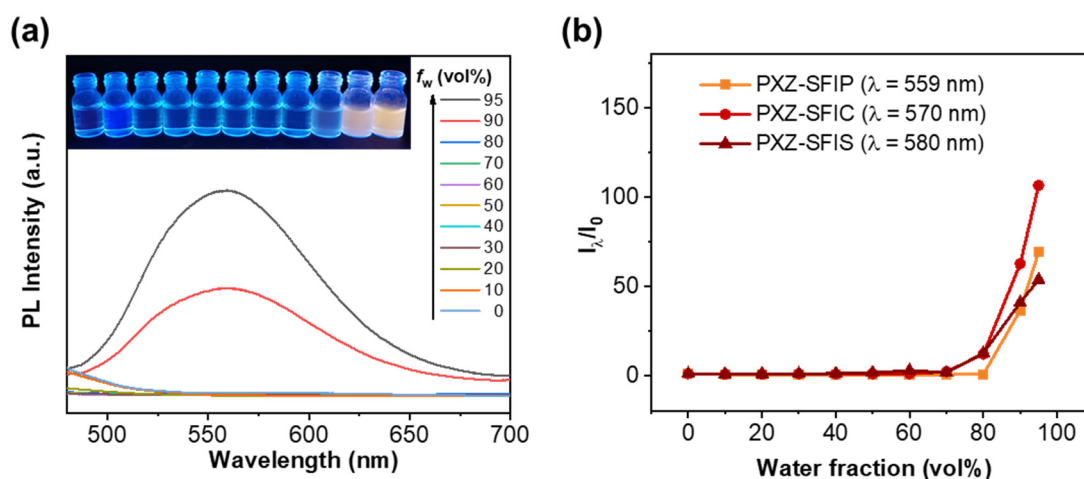


**Figure 3.** (a) PL spectra of **PXZ-SFIP** in THF/water mixtures with different water fractions; inset: photograph of the samples in sequence under excitation of 365 nm. (b) Plot of  $I_{\lambda} \text{ nm}/I_0$  versus water fraction of the solvent mixture, where  $I_0$  is the PL intensity in pure THF solution,  $\lambda$  is the peak wavelengths detailed in the legend.

Experimental excited state energies were measured by fluorescent and phosphorescent spectroscopy in film state, as an imitation of the environment in emissive layers (EML) of OLEDs. Here, *bis*[2-(diphenylphosphino)phenyl] ether oxide (DPEPO) was selected as host material due to its large energy band gap and high  $T_1$  level ( $\sim 3.4$  eV). As shown in Figure 4,  $S_1$  and  $T_1$  levels of the emitters were estimated from the onset of fluorescent and phosphorescent spectra, giving the values of 2.61/2.59 eV for **PXZ-SFIP**, 2.54/2.52 eV for **PXZ-SFIC**, and 2.51/2.48 eV for **PXZ-SFIS**. The small  $\Delta E_{STs}$  around 0.02–0.03 eV were consistent with the previous theoretical calculation results, assuring an effective up-conversion process from  $T_1$  to  $S_1$ . To confirm their TADF character, the transient PL decay profiles of the three emitters were recorded in both solution and doped films. The samples in degassed toluene displayed obvious delayed components that could be largely quenched in aerated conditions due to the sensitivity of the triplet state excitons to oxygen (Figure S5). Meanwhile, the transient PL curves of 10 wt% doped DPEPO films could also be fitted with biexponential functions, with prompt and delayed fluorescence lifetimes ( $\tau_p/\tau_d$ ) of 30.5 ns/1.2  $\mu$ s, 28.7 ns/1.3  $\mu$ s, and 29.9 ns/1.2  $\mu$ s for **PXZ-SFIP**, **PXZ-SFIC**, and **PXZ-SFIS**, separately, and the ratios of the delayed fluorescence were 64.4%, 62.3%, and 61.3%. The absolute photoluminescent quantum yield ( $\Phi_{PL}$ ) of the DPEPO films doped with the TADF emitters was found to be 52%/41%/21% for **PXZ-SFIP/PXZ-SFIC/PXZ-SFIS**.

Subsequently, the  $S_1 \rightarrow S_0$  radiative and nonradiative decay rate constants ( $k_{r,S}$ ,  $k_{nr,S}$ ) together with the ISC ( $k_{ISC}$ ) and RISC rate constants ( $k_{RISC}$ ) were extrapolated to provide more in-depth information on the TADF characteristics and PL efficiencies (Table 3). The emitters shared comparable  $k_{ISC}$  and  $k_{RISC}$  values due to similar  $\Delta E_{STs}$ , noting that all  $k_{RISCs}$  were at the state-of-the-art level of  $\sim 10^6 \text{ s}^{-1}$  to guarantee effective utilization of triplet excitons. On the contrary, the  $k_{r,S}$  values decreased significantly from  $6.1/5.4 \times 10^6 \text{ s}^{-1}$  of **PXZ-SFIP/PXZ-SFIC** to  $2.7 \times 10^6 \text{ s}^{-1}$  of **PXZ-SFIS**, in line with the trend of theoretically predicted oscillator strengths. The **PXZ-SFIS** also possessed the largest  $k_{nr,S}$  in these emitters, with this value even outcompeting its  $k_{r,S}$ , manifesting considerable nonradiative dissipation of excitons through internal conversion with its more stabilized CT energy as governed by the energy-gap law.

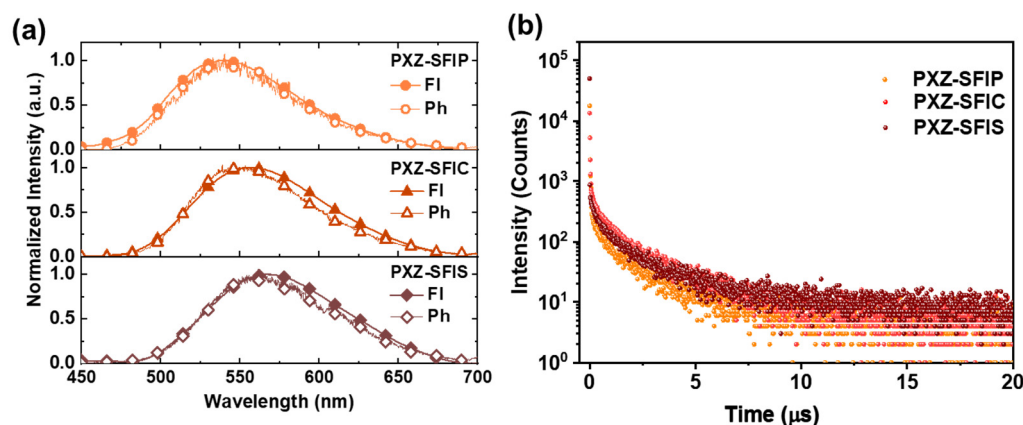


**Figure 4.** (a) Steady-state emission (FI) spectra and phosphorescence (Ph) spectra of **PXZ-SFIP**, **PXZ-SFIC**, and **PXZ-SFIS** doped in CBP thin film (10 wt%), measured at 77 K. (b) Transient PL decay curves of DPEPO thin films doped with 10 wt% of **PXZ-SFIP**, **PXZ-SFIC**, and **PXZ-SFIS** emitters.

**Table 3.** Photophysical parameters of 10 wt% doped DPEPO films of the TADF compounds.

| Compound        | $\Phi_{\text{PL}}$<br>(%) | $\tau_{\text{PF}}$<br>(ns) | $\tau_{\text{DF}}$<br>(μs) | $k_{\text{r,S}}$<br>( $\times 10^6 \text{ s}^{-1}$ ) | $k_{\text{nr,S}}$<br>( $\times 10^6 \text{ s}^{-1}$ ) | $k_{\text{ISC}}$<br>( $\times 10^7 \text{ s}^{-1}$ ) | $k_{\text{RISC}}$<br>( $\times 10^6 \text{ s}^{-1}$ ) |
|-----------------|---------------------------|----------------------------|----------------------------|--|---|--|---|
| <b>PXZ-SFIP</b> | 52.0                      | 30.5                       | 1.2                        | 6.1  | 5.6   | 2.1  | 2.4   |
| <b>PXZ-SFIC</b> | 41.0                      | 28.7                       | 1.3                        | 5.4  | 7.8   | 2.2  | 2.1   |
| <b>PXZ-SFIS</b> | 21.0                      | 29.9                       | 1.2                        | 2.7  | 10.2  | 2.1  | 2.2   |

### 3.5. Device Characterization

Electroluminescent properties of the TADF emitters were further evaluated by OLEDs with the TADF emitter doped films as the light-emitting layer. The devices adopted the configuration of ITO/HATCN (5 nm)/TAPC (10 nm)/mCP (10 nm)/DPEPO: 10 wt% TADF emitter (20 nm)/DPEPO (10 nm)/Liq (1.5 nm)/Al (100 nm) (Figure 5a). Here, 1,4,5,8,9,11-hexaazatriphenylenehexacarbonitrile (HATCN) and 8-hydroxyquinolinolito-lithium (Liq) were used as the hole injection layer (HIL) and electron injection layer (EIL), respectively. 1,1-Bis[(di-4-tolylamino)phenyl]cyclohexane (TAPC) and 1,3,5-Tris(3-pyridyl-3-phenyl)benzene (TmPyPB) served as the hole transport layer (HTL) and electron-transporting layer (ETL), respectively. 1,3-Di(9H-carbazol-9-yl)benzene (mCP) and DPEPO were applied as exciton-blocking layers (EBL). DPEPO was selected as the host material in the emitting layer (EML) with its sufficiently high  $T_1$  energy to avoid energy back transfer.

In 10 wt% doped devices, the EL spectra clearly originated from the TADF emitters, suggesting complete energy transfer from DPEPO host to dopants. The devices displayed yellow to orange emissions peaking at 553 nm for **PXZ-SFIP**, 572 nm for **PXZ-SFIC**, and 584 nm **PXZ-SFIS**, respectively. **PXZ-SFIP** with the highest  $\Phi_{\text{PL}}$  exhibited the best device performance with the maximum external quantum efficiency ( $\text{EQE}_{\text{max}}$ ) of 5.75%, current efficiency ( $\text{CE}_{\text{max}}$ ) of 17.06  $\text{cd} \cdot \text{A}^{-1}$ , and power efficiency ( $\text{PE}_{\text{max}}$ ) of 13.40  $\text{lm} \cdot \text{W}^{-1}$ . Comparatively, devices based on **PXZ-SFIC** and **PXZ-SFIS** showed slightly inferior efficiencies with maximum EQE values at 3.17% and 1.30%, separately, which could be well explained by their suppressed singlet radiative transition and faster non-radiative internal conversion process. It is noteworthy that the devices did not come across serious efficiency roll-off at high brightness, attributing to the emitters' AIE character, i.e., the efficiency roll-off value of the **PXZ-SFIP** device was only 16.7% at 1000  $\text{cd} \cdot \text{m}^{-2}$ . Additionally, the shortened  $\tau_{\text{DFS}}$  and efficient RISC process may also suppress notorious triplet-triplet annihilation (TTA), singlet-triplet annihilation (STA), or triplet polaron exciton annihilation. The EL data for all the emitters are summarized in Table 4.

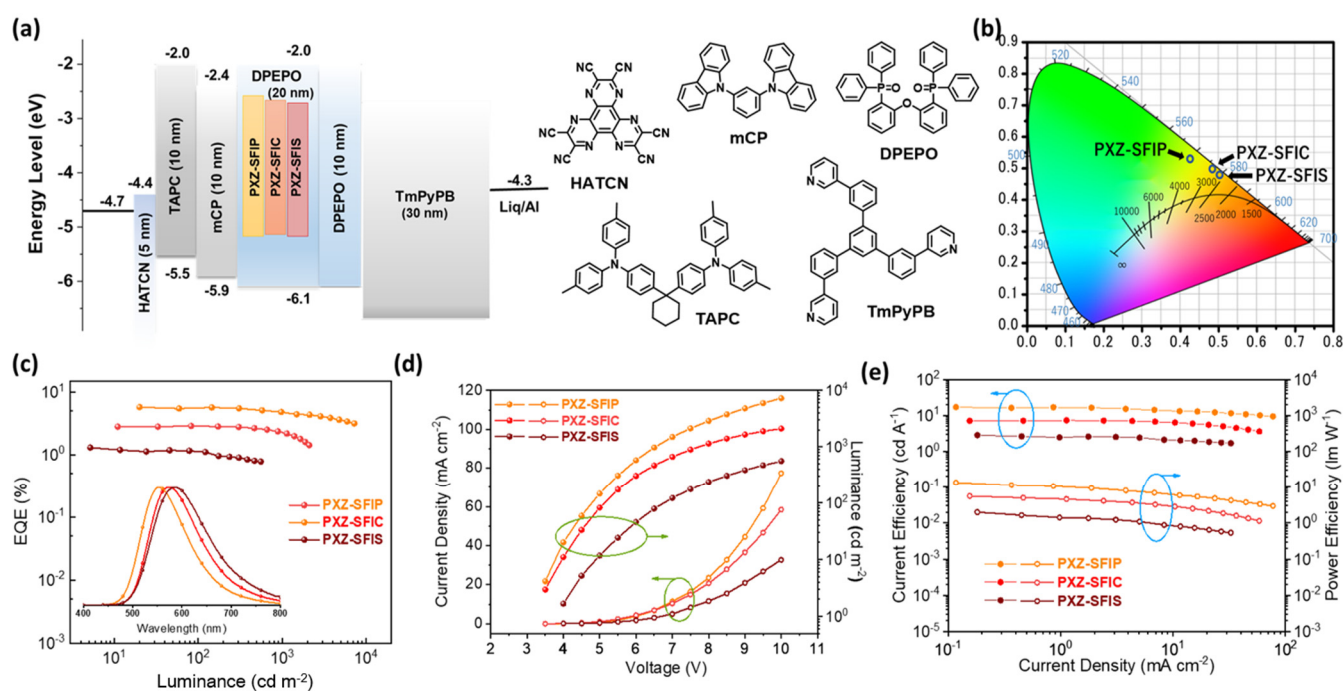


**Figure 5.** (a) Energy level alignment of all the materials used in the current study (left) and schematic diagrams of the basic structures of the quadruple-layer device (right). (b) The Commission Internationale de l’Eclairage coordinates recorded at maximum EQE (c) External quantum efficiency (EQE) versus current density ( $J$ ); inset: normalized EL spectra of the devices. (d) Current density–voltage ( $J$ – $V$ ) and luminance–voltage ( $L$ – $V$ ) characteristics of the devices. (e) Power efficiency (PE) and current efficiency (CE) versus current density ( $J$ ).

**Table 4.** Summary of device performances.

| Emitter  | $V_{on}^a$<br>(V) | $CE_{max}^b$<br>( $cd A^{-1}$ ) | $PE_{max}^b$<br>( $lm W^{-1}$ ) | EQE <sup>b</sup><br>(%) | EL <sub>peak</sub><br>(nm) | CIE <sup>c</sup><br>(x,y) |
|----------|-------------------|---------------------------------|---------------------------------|-------------------------|----------------------------|---------------------------|
| PXZ-SFIP | 3.5               | 17.06                           | 13.40                           | 5.75/5.58/4.79          | 553                        | (0.42, 0.54)              |
| PXZ-SFIC | 3.5               | 8.01                            | 7.19                            | 3.17/2.89/2.27          | 572                        | (0.48, 0.50)              |
| PXZ-SFIS | 4.0               | 2.85                            | 1.99                            | 1.30/1.14/-             | 584                        | (0.50, 0.48)              |

<sup>a</sup> Turn-on voltage (at a brightness of  $1 cd \cdot m^{-2}$ ); <sup>b</sup> the maximum CE (current efficiency), the maximum PE (power efficiency); EQE (external quantum efficiency): maximum, values at  $100 cd \cdot m^{-2}$ , and  $1000 cd \cdot m^{-2}$ ; <sup>c</sup> CIE: Commission Internationale de l’Eclairage chromaticity coordinates.

#### 4. Conclusions

In summary, a series of TADF emitters were constructed by 10*H*-phenoxazine and novel dibenzothiophene sulfoximine derivatives. By attaching diphenylphosphoryl, benzoyl, and benzenesulfonyl units with gradually increased electron deficiencies at the secondary amine in dibenzothiophene sulfoximine acceptors, bathochromic shifted fluorescence from yellow to orange were obtained with more stabilized CT energy. The orthogonal D–A conformation endowed these emitters nearly degenerate  $S_1$  and  $T_1$  state, high  $k_{RISC}$  at the level of  $\sim 10^6 s^{-1}$ , and efficient delayed fluorescence. At the same time, the emitters manifested distinct AIE properties with  $\Phi_{PL}$  up to 52% in film state. Subsequently, devices based on **PXZ-SFIP** as emitting material realized a maximum EQE of 5.8% with reduced efficiency roll-off. This work not only demonstrates dibenzothiophene sulfoximine as potential construction units for AIE-active TADF emitters, but also provides a meaningful strategy for designing color-managing acceptors.

**Supplementary Materials:** The following are available online, Figure S1: The thermogravimetric analysis (TGA) plots of PXZ-SFIS, PXZ-SFIC and PXZ-SFIP under  $N_2$  stream (flow rate:  $20 mL \cdot min^{-1}$ ; heating rate:  $10 ^\circ C \cdot min^{-1}$ ), Figure S2: DSC thermograms (second heating cycle) of PXZ-SFIS, PXZ-

**SFIC** and **PXZ-SFIP** under N<sub>2</sub> stream (flow rate: 20 mL min<sup>-1</sup>; heating rate: 10 °C min<sup>-1</sup>), Figure S3: Cyclic voltammograms of **PXZ-SFIP**, **PXZ-SFIC**, and **PXZ-SFIS** in 1×10<sup>-3</sup> M dichloromethane, Figure S4: PL spectra of (a) **PXZ-SFIC** and (b) **PXZ-SFIS** in THF/H<sub>2</sub>O mixed solvents with different water volume fractions, Figure S5: Transient PL decay curves of **PXZ-SFIP**, **PXZ-SFIC**, and **PXZ-SFIS** in 1×10<sup>-5</sup> M toluene solution, Table S1: Natural transition orbitals (NTO) in the S<sub>1</sub> and T<sub>1</sub> states of the TADF emitters, Table S2: Thermal analysis of the three compounds.

**Author Contributions:** Y.Y., R.X., X.C., Z.C., X.L., Y.Z. (Youming Zhang), S.G., Y.Z. (Yang Zou) and C.Y. contributed to methodology and writing of the paper. All authors have read and agreed to the published version of the manuscript.

**Funding:** This research received no external funding.

**Institutional Review Board Statement:** Not applicable.

**Informed Consent Statement:** Not applicable.

**Data Availability Statement:** Data on the compounds are available from the authors.

**Acknowledgments:** We gratefully acknowledge the financial support from the Natural Science Foundation of China (Grant Nos. 51903159 and 51903157), the Shenzhen Science and Technology Program (KQTD20170330110107046) and the Natural Science Foundation of Shenzhen University (Grant No. 2019001). We thank the Instrumental Analysis Center of Shenzhen University for analytical support.

**Conflicts of Interest:** The authors declare no conflict of interest.

**Sample Availability:** Samples of the compounds are available from the authors.

## References

1. Endo, A.; Sato, K.; Yoshimura, K.; Kai, T.; Kawada, A.; Miyazaki, H.; Adachi, C. Efficient up-conversion of triplet excitons into a singlet state and its application for organic light emitting diodes. *Appl. Phys. Lett.* **2011**, *98*, 083302.
2. dos Santos, P.L.; Etherington, M.K.; Monkman, A.P. Chemical and conformational control of the energy gaps involved in the thermally activated delayed fluorescence mechanism. *J. Mater. Chem. C* **2018**, *6*, 4842–4853.
3. Zhang, Q.; Li, B.; Huang, S.; Nomura, H.; Tanaka, H.; Adachi, C. Efficient blue organic light-emitting diodes employing thermally activated delayed fluorescence. *Nat. Photonics* **2014**, *8*, 326–332.
4. Zou, Y.; Gong, S.; Xie, G.; Yang, C. Design Strategy for Solution-Processable Thermally Activated Delayed Fluorescence Emitters and Their Applications in Organic Light-Emitting Diodes. *Adv. Opt. Mater.* **2018**, *6*, 1800568.
5. Zhang, D.; Song, X.; Cai, M.; Duan, L. Blocking Energy-Loss Pathways for Ideal Fluorescent Organic Light-Emitting Diodes with Thermally Activated Delayed Fluorescent Sensitizers. *Adv. Mater.* **2018**, *30*, 1705250.
6. Tao, Y.; Yuan, K.; Chen, T.; Xu, P.; Li, H.; Chen, R.; Zheng, C.; Zhang, L.; Huang, W. Thermally Activated Delayed Fluorescence Materials Towards the Breakthrough of Organoelectronics. *Adv. Mater.* **2014**, *26*, 7931–7958.
7. Uoyama, H.; Goushi, K.; Shizu, K.; Nomura, H.; Adachi, C. Highly efficient organic light-emitting diodes from delayed fluorescence. *Nature* **2012**, *492*, 234–238.
8. Goushi, K.; Yoshida, K.; Sato, K.; Adachi, C. Organic light-emitting diodes employing efficient reverse intersystem crossing for triplet-to-singlet state conversion. *Nat. Photonics* **2012**, *6*, 253–258.
9. Hirata, S.; Sakai, Y.; Masui, K.; Tanaka, H.; Lee, S.Y.; Nomura, H.; Nakamura, N.; Yasumatsu, M.; Nakanotani, H.; Zhang, Q. Highly efficient blue electroluminescence based on thermally activated delayed fluorescence. *Nat. Mater.* **2015**, *14*, 330–336.
10. Liu, Y.; Li, C.; Ren, Z.; Yan, S.; Bryce, M.R. All-organic thermally activated delayed fluorescence materials for organic light-emitting diodes. *Nat. Rev. Mater.* **2018**, *3*, 18020.
11. He, J.; He, Y.; Chen, Y.; Zhang, X.; Hu, C.; Zhuang, J.; Lei, B.; Liu, Y. Construction and multifunctional applications of carbon dots/PVA nanofibers with phosphorescence and thermally activated delayed fluorescence. *Chem. Eng. J.* **2018**, *347*, 505–513.
12. Shizu, K.; Noda, H.; Tanaka, H.; Taneda, M.; Uejima, M.; Sato, T.; Tanaka, K.; Kaji, H.; Adachi, C. Highly efficient blue electroluminescence using delayed-fluorescence emitters with large overlap density between luminescent and ground states. *J. Phys. Chem. C* **2015**, *119*, 26283–26289.
13. Yu, L.; Wu, Z.; Xie, G.; Zhong, C.; Zhu, Z.; Cong, H.; Ma, D.; Yang, C. Achieving a balance between small singlet–triplet energy splitting and high fluorescence radiative rate in a quinoxaline-based orange-red thermally activated delayed fluorescence emitter. *Chem. Commun.* **2016**, *52*, 11012–11015.
14. Yang, Z.; Mao, Z.; Xie, Z.; Zhang, Y.; Liu, S.; Zhao, J.; Xu, J.; Chi, Z.; Aldred, M.P. Recent advances in organic thermally activated delayed fluorescence materials. *Chem. Soc. Rev.* **2017**, *46*, 915–1016.
15. Dias, F.B.; Penfold, T.J.; Monkman, A.P. Photophysics of thermally activated delayed fluorescence molecules. *Methods Appl. Fluoresc.* **2017**, *5*, 012001.

16. Im, Y.; Kim, M.; Cho, Y.J.; Seo, J.-A.; Yook, K.S.; Lee, J.Y. Molecular Design Strategy of Organic Thermally Activated Delayed Fluorescence Emitters. *Chem. Mater.* **2017**, *29*, 1946–1963.
17. Bronstein, H.; Nielsen, C.B.; Schroeder, B.C.; McCulloch, I. The role of chemical design in the performance of organic semiconductors. *Nat. Rev. Chem.* **2020**, *4*, 66–77.
18. Higginbotham, H.F.; Yi, C.-L.; Monkman, A.P.; Wong, K.-T. Effects of Ortho-Phenyl Substitution on the rISC Rate of D–A Type TADF Molecules. *J. Phys. Chem. C* **2018**, *122*, 7627–7634.
19. Godumala, M.; Yoon, J.; Park, S.Y.; Lee, C.; Kim, Y.; Jeong, J.-E.; Park, S.; Woo, H.Y.; Cho, M.J.; Choi, D.H. 5H-Benzo[d]Benzo[4,5]Imidazo[2,1-b][1,3]Thiazine as a Novel Electron-Acceptor Cored High Triplet Energy Bipolar Host Material for Efficient Solution-Processable Thermally Activated Delayed Fluorescence Organic Light-Emitting Diodes. *Front. Chem.* **2020**, *8*, <https://doi.org/10.3389/fchem.2020.00061>.
20. Cai, X.; Su, S.-J. Marching Toward Highly Efficient, Pure-Blue, and Stable Thermally Activated Delayed Fluorescent Organic Light-Emitting Diodes. *Adv. Funct. Mater.* **2018**, *28*, 1802558.
21. Wu, K.; Zhang, T.; Wang, Z.; Wang, L.; Zhan, L.; Gong, S.; Zhong, C.; Lu, Z.-H.; Zhang, S.; Yang, C. De Novo Design of Excited-State Intramolecular Proton Transfer Emitters via a Thermally Activated Delayed Fluorescence Channel. *J. Am. Chem. Soc.* **2018**, *140*, 8877–8886.
22. Xiang, Y.; Zhao, Y.; Xu, N.; Gong, S.; Ni, F.; Wu, K.; Luo, J.; Xie, G.; Lu, Z.-H.; Yang, C. Halogen-induced internal heavy-atom effect shortening the emissive lifetime and improving the fluorescence efficiency of thermally activated delayed fluorescence emitters. *J. Mater. Chem. C* **2017**, *5*, 12204–12210.
23. Chen, J.X.; Tao, W.W.; Chen, W.C.; Xiao, Y.F.; Wang, K.; Cao, C.; Yu, J.; Li, S.; Geng, F.X.; Adachi, C. Red/Near-Infrared Thermally Activated Delayed Fluorescence OLEDs with Near 100% Internal Quantum Efficiency. *Angew. Chem. Int. Ed.* **2019**, *58*, 14660–14665.
24. Zhang, Y.L.; Ran, Q.; Wang, Q.; Liu, Y.; Hänisch, C.; Reineke, S.; Fan, J.; Liao, L.S. High-Efficiency Red Organic Light-Emitting Diodes with External Quantum Efficiency Close to 30% Based on a Novel Thermally Activated Delayed Fluorescence Emitter. *Adv. Mater.* **2019**, *31*, 1902368.
25. Pathak, S.K.; Xiang, Y.; Huang, M.; Huang, T.; Cao, X.; Liu, H.; Xie, G.; Yang, C. Fused tetracyclic tris[1,2,4]triazolo[1,3,5]triazine as a novel rigid electron acceptor for efficient thermally activated delayed fluorescence emitters. *RSC Adv.* **2020**, *10*, 15523–15529.
26. Cao, X.; Zhang, D.; Zhang, S.; Tao, Y.; Huang, W. CN-Containing donor–acceptor-type small-molecule materials for thermally activated delayed fluorescence OLEDs. *J. Mater. Chem. C* **2017**, *5*, 7699–7714.
27. Kim, J.H.; Yun, J.H.; Lee, J.Y. Recent Progress of Highly Efficient Red and Near-Infrared Thermally Activated Delayed Fluorescent Emitters. *Adv. Opt. Mater.* **2018**, *6*, 1800255.
28. Xiao, R.; Xiang, Y.; Cao, X.; Li, N.; Huang, T.; Zhou, C.; Zou, Y.; Xie, G.; Yang, C. Star-shaped thermally activated delayed fluorescence emitters with a tri-armed arylsulfonic acceptor for efficient solution processed organic light emitting diodes. *J. Mater. Chem. C* **2020**, *8*, 5580–5586.
29. Wang, Y.; Zhang, Y.; Hu, W.; Quan, Y.; Li, Y.; Cheng, Y. Circularly Polarized Electroluminescence of Thermally Activated Delayed Fluorescence-Active Chiral Binaphthyl-Based Luminogens. *ACS Appl. Mater. Interfaces* **2019**, *11*, 26165–26173.
30. Matsuoka, K.; Albrecht, K.; Nakayama, A.; Yamamoto, K.; Fujita, K. Highly Efficient Thermally Activated Delayed Fluorescence Organic Light-Emitting Diodes with Fully Solution-Processed Organic Multilayered Architecture: Impact of Terminal Substitution on Carbazole–Benzophenone Dendrimer and Interfacial Engineering. *ACS Appl. Mater. Interfaces* **2018**, *10*, 33343–33352.
31. Xu, J.; Zhu, X.; Guo, J.; Fan, J.; Zeng, J.; Chen, S.; Zhao, Z.; Tang, B.Z. Aggregation-Induced Delayed Fluorescence Luminogens with Accelerated Reverse Intersystem Crossing for High-Performance OLEDs. *ACS Mater. Lett.* **2019**, *1*, 613–619.
32. Im, Y.; Han, S.H.; Lee, J.Y. Deep blue thermally activated delayed fluorescent emitters using CN-modified indolocarbazole as an acceptor and carbazole-derived donors. *J. Mater. Chem. C* **2018**, *6*, 5012–5017.
33. Wong, M.Y.; Krotkus, S.; Copley, G.; Li, W.; Murawski, C.; Hall, D.; Hedley, G.J.; Jaricot, M.; Cordes, D.B.; Slawin, A.M.Z.; et al. Deep-Blue Oxadiazole-Containing Thermally Activated Delayed Fluorescence Emitters for Organic Light-Emitting Diodes. *ACS Appl. Mater. Interfaces* **2018**, *10*, 33360–33372.
34. Chan, C.Y.; Cui, L.S.; Kim, J.U.; Nakanotani, H.; Adachi, C. Rational Molecular Design for Deep-Blue Thermally Activated Delayed Fluorescence Emitters. *Adv. Funct. Mater.* **2018**, *28*, 1706023.
35. Lin, C.-C.; Huang, M.-J.; Chiu, M.-J.; Huang, M.-P.; Chang, C.-C.; Liao, C.-Y.; Chiang, K.-M.; Shiao, Y.-J.; Chou, T.-Y.; Chu, L.-K.; et al. Molecular Design of Highly Efficient Thermally Activated Delayed Fluorescence Hosts for Blue Phosphorescent and Fluorescent Organic Light-Emitting Diodes. *Chem. Mater.* **2017**, *29*, 1527–1537.
36. Gibson, J.; Monkman, A.P.; Penfold, T.J. The Importance of Vibronic Coupling for Efficient Reverse Intersystem Crossing in Thermally Activated Delayed Fluorescence Molecules. *ChemPhysChem* **2016**, *17*, 2956–2961.
37. Xie, G.; Luo, J.; Huang, M.; Chen, T.; Wu, K.; Gong, S.; Yang, C. Inheriting the Characteristics of TADF Small Molecule by Side-Chain Engineering Strategy to Enable Bluish-Green Polymers with High PLQYs up to 74% and External Quantum Efficiency over 16% in Light-Emitting Diodes. *Adv. Mater.* **2017**, *29*, 1604223.
38. Neena, K.K.; Sudhakar, P.; Thilagar, P. Catalyst- and Template-Free Ultrafast Visible-Light-Triggered Dimerization of Vinylpyridine-Functionalized Tetraarylamino borane: Intriguing Deep-Blue Delayed Fluorescence. *Angew. Chem. Int. Ed.* **2018**, *57*, 16806–16810.
39. Bunzmann, N.; Weissenseel, S.; Kudriashova, L.; Gruene, J.; Krugmann, B.; Grazulevicius, J.V.; Sperlich, A.; Dyakonov, V. Optically and electrically excited intermediate electronic states in donor:acceptor based OLEDs. *Mater. Horiz.* **2020**, *7*, 1126–1137.

40. Zeng, W.; Lai, H.Y.; Lee, W.K.; Jiao, M.; Shiu, Y.J.; Zhong, C.; Gong, S.; Zhou, T.; Xie, G.; Sarma, M.; et al. Achieving Nearly 30% External Quantum Efficiency for Orange-Red Organic Light Emitting Diodes by Employing Thermally Activated Delayed Fluorescence Emitters Composed of 1,8-Naphthalimide-Acridine Hybrids. *Adv. Mater.* **2018**, *30*, 1704961.
41. Lücking, U. Sulfoximines: A Neglected Opportunity in Medicinal Chemistry. *Angew. Chem. Int. Ed.* **2013**, *52*, 9399–9408.
42. Wiezorek, S.; Lamers, P.; Bolm, C. Conversion and degradation pathways of sulfoximines. *Chem. Soc. Rev.* **2019**, *48*, 5408–5423.
43. Bizet, V.; Hendriks, C.M.; Bolm, C. Sulfur imidations: Access to sulfimides and sulfoximines. *Chem. Soc. Rev.* **2015**, *44*, 3378–3390.
44. Cao, X.; Chen, Z.; Gong, S.; Pan, K.; Zhou, C.; Huang, T.; Chai, D.; Zhan, Q.; Li, N.; Zou, Y.; et al. Designing Versatile Sulfoximine as Accepting Unit to Regulate the Photophysical Properties of TADF Emitters towards High-performance OLEDs. *Chem. Eng. J.* **2020**, *399*, 125648.
45. Huang, B.; Chen, W.-C.; Li, Z.; Zhang, J.; Zhao, W.; Feng, Y.; Tang, B.Z.; Lee, C.-S. Manipulation of Molecular Aggregation States to Realize Polymorphism, AIE, MCL, and TADF in a Single Molecule. *Angew. Chem. Int. Ed.* **2018**, *57*, 12473–12477.